Article

Theoretical Evaluation of the Interactions between Metal-Phthalocyanines and Various Fullerenes as Delivery Systems

Oana-Raluca Pop [1],[*] and Jacobus (Koos) Frederick Van Staden [2]

[1] Faculty of Pharmacy, University of Medicine and Pharmacy "Victor Babeş" Timisoara, Eftimie Murgu Square 2, 300041 Timisoara, Romania
[2] National Institute of Research for Electrochemistry and Condensed Matter, 202, Splaiul Independentei Str., 060021 Bucharest, Romania
[*] Correspondence: pop.raluca@umft.ro

Abstract: The photodynamic therapy (PDT) represents a non-invasive method with good results in the treatment of superficial tumors. PDT is based on a combination of two factors, namely, a non-toxic photosensitizing molecule and a light source; the photosensitizer absorbs a photon of radiation, leading to a series of reactions that cause irreversible damage to the affected tissue. The present paper investigates the photosensitization properties of nine substituted metal-phthalocyanines (the central metals being iron, nickel, and zinc). In addition, the interactions between the aforementioned compounds and four fullerenes are investigated by means of molecular docking studies in order to verify their potential as delivery systems for phthalocyanines. Our results outline that the properties of metal-phthalocyanines are mainly influenced by the type of substituent and to a lesser extent by the nature of the metal. The binding energies of the metal-phthalocyanines towards the fullerenes suggest a slight increased affinity for the fullerene C_{52} as compared to the three nitrogen- and phosphorus-doped $C_{46}N_3P_3$ fullerenes.

Keywords: metal-phthalocyanine; fullerenes; delivery system; ab initio

1. Introduction

Photodynamic therapy involves the marking of diseased tissue with a photosensitizer followed by exposure to light (the wavelength is generally in visible spectrum) to induce a phototoxic reaction which leads to its destruction. The main field of application of photodynamic therapy is oncology. Photosensitizers preferentially accumulate in neoplastic tissues, allowing a priori selective destruction of tumors [1,2].

Phthalocyanines are promising photosensitizers for photodynamic therapy (PDT) due to their strong absorption of red light that penetrates tissues, easy derivatization, and high singlet oxygen generation efficiency [3]. Three classes of metallophthalocyanines have been used in clinical trials, namely, silicon (IV) phthalocyanine [4,5], zinc (II) phthalocyanine [6], and aluminum (III) phthalocyanine [7]. However, the main problems with phthalocyanine derivatives are their low solubility in biological environments and poor retention in malignant tissues [8]. The study of their photosensitization properties in a heterogeneous environment and the evaluation of their interactions with biological molecules and cellular components have thus received increased interest [8]. The application of computational chemistry methods can provide necessary information on the stability and reactivity of these compounds.

Zhang et al. [9] used DFT methods to investigate the structure and spectroscopic properties of phthalocyanines substituted by methoxy and sulfoxyl groups. In addition, theoretical chemistry methods have been used to study zinc phthalocyanines with grafted naphthoxy and phenylazonaftoxy moieties [10] as well as phthalocyanines substituted with

four imidazolyl rings [11]. The efficiency of certain symmetrical (substituted with four tert-butyl residues) and asymmetrical (substituted with three tert-butyl residues and an iodine group) phthalocyanines as photosensitizers was investigated in [12]. Symmetrically substituted phthalocyanines have been shown to be effective in PDT applied to the lung, intestine, ovarian, and pancreatic tumors, while asymmetrically substituted phthalocyanines are promising imaging agents for colon and pancreatic tumors [12]. In [13], the authors outlined the high biological activity of fluorinated phthalocyanines, with their results showing complete regression of tumors in 20% of treated mice.

Another area of interest is represented by the study of delivery systems based on colloidal structures due to their potential for transporting different drugs while protecting them against degradation. Drug delivery systems with adjustable properties have the ability to host a variety of molecules. For example, vesicularly cross-linked hydrogels are able to provide different environments for pharmaceuticals comprising bulk water, sites on polymeric chains, the interior of vesicles, and bilayers [14]. Most phthalocyanines are hydrophobic compounds that require association with other drug delivery systems. A number of phthalocyanines derivatized with chlorine and aluminum have shown promising results in PDT, producing high concentrations of reactive oxygen species. These results have been confirmed by a series of in vitro tests on A549 cancer lines, showing high phototoxicity [15]. Pyridine derivatives are a type of important pharmaceutical intermediates which have excellent biocompatibility; they can form hydrogen bonds with biological molecules thanks to the presence of a nitrogen atom. Thus, [16] investigated the in vitro photodynamic activity of Zn (II) phthalocyanines substituted with pyridine groups. Other results have shown that a tetrasubstituted zinc phthalocyanine has a low tendency to aggregate in the biological environment and a high level of reactive oxygen species, giving it high photodynamic activity [17].
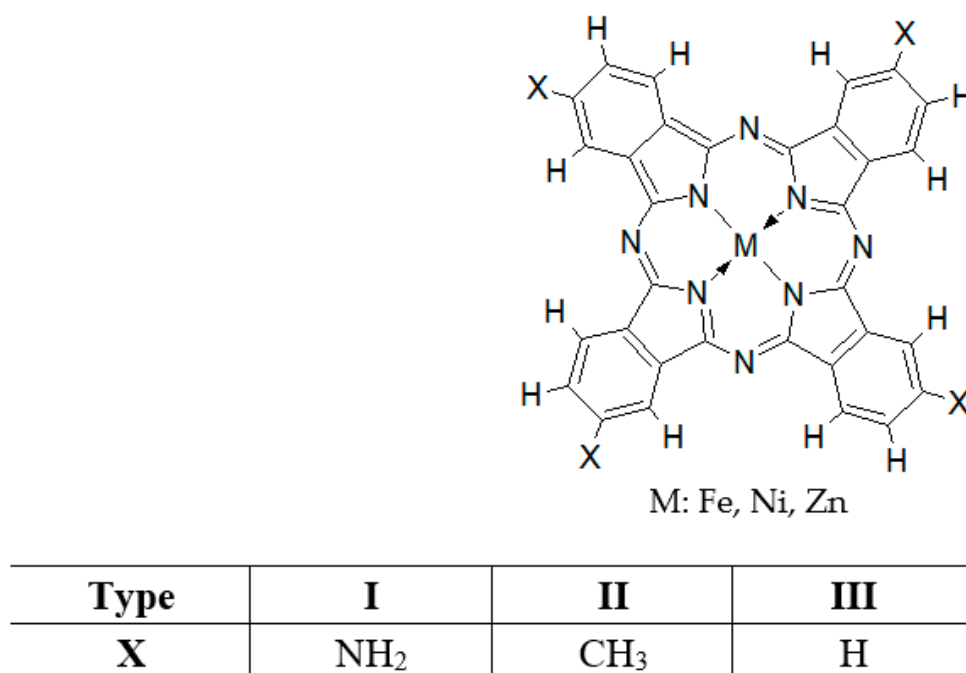
The present study deals with the investigation of variously substituted metal-phthalocyanines (with amino and methyl groups) as possible photosensitizers, the central metal being Fe, Ni, and Zn, respectively. In the following, amino-substituted phthalocyanines are denoted by I, methyl derivatives are denoted by II, and unsubstituted phthalocyanines by III. According to data from the literature, a compound with applications in photodynamic therapy is characterized by the following properties [18]: low HOMO orbital energy (which is an advantage for electronic transfer); a small HOMO–LUMO gap; low dipole moment; and UV–Vis absorption in the range of 400–650 nm.

The general structure of the investigated metal-phthalocyanines is depicted in the Figure 1.

The second part of this study deals with the evaluation of four fullerenes as nanocarriers for these phthalocyanines. We employed an all-carbon fullerene (C_{52}) and three fullerenes doped with nitrogen and phosphorus atoms ($C_{46}N_3P_3$) with different substitution patterns. The heteroatomic substitution pattern is depicted below for both sumanene, a circulene-type precursor of fullerene C_{52}, and the corresponding fullerenes. Our previous studies have dealt with the evaluation of the properties and aromatic characteristics of various all-carbon and nitrogen- and phosphorus-doped nanostructures, including both fullerenes and their polycyclic aromatic hydrocarbon (mostly coronene and sumanene) precursors [19,20].

The heteroatom substitution pattern is illustrated in Figure 2.

The present paper aims to (i) evaluate the properties of nine metal-phthalocyanines in order to establish whether they are suitable photosensitizers and (ii) investigate the interactions between the aforementioned compounds and several heteroatom-doped fullerenes in order to use the latter compounds as delivery systems. Both the influence of the central metal and the role of the substituents on the properties of the title compounds are evaluated.

Figure 1. General structure of the studied metal-phthalocyanines.

Type	I	II	III
X	NH_2	CH_3	H

Sumanene

Sumanene (A)

Sumanene (B)

Sumenene (C)

C_{52}

$C_{46}N_3P_3$ (A)

$C_{46}N_3P_3$ (B)

$C_{46}N_3P_3$ (C)
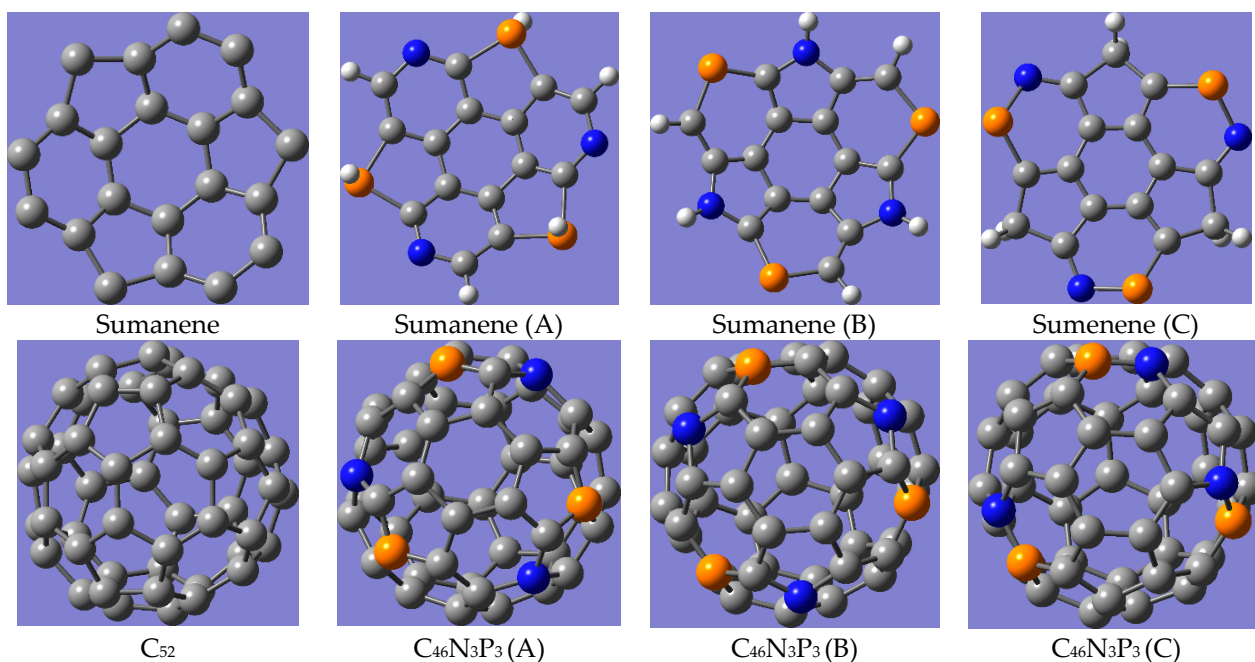
Figure 2. Fullerenes investigated as delivery systems for the metal-phthalocyanins. (C atoms—grey, N atoms—blue, P atoms—orange).

2. Materials and Methods

The phthalocyanines were first optimized at the semi-empirical level (PM6 method implemented in Gaussian 09W), and the obtained structures were refined at the HF/LanL2DZ level of theory. A similar approach was employed for the four fullerenes. These computations were performed by means of G09W software [21]. In addition, the energies of the HOMO and LUMO orbitals and the dipole moment were computed by means of G09 W at the HF/LanL2DZ level of theory.

Chemical potential (μ), chemical hardness (η), and electrophilicity (ω) were calculated using the following equations:

$$\mu = -1/2(E_{LUMO} + E_{HOMO}); \eta = 1/2(E_{LUMO} - E_{HOMO}); \omega = \mu^2/2\eta$$

The steric parameters [22], namely, ovality, Connolly accessible area, and Connolly solvent excluded volume, as well as the partition coefficient logP, were obtained with Chem3D software. Chem3D was employed for the computations of the number of hydrogen bond donors and acceptors as well. AutoDock Vina software [23] was employed for the molecular docking studies.

The fullerenes were considered as receptors and a grid box of $40 \times 40 \times 40$ Å was used, with the center of the grid box considered the center of the fullerenes. The optimized structures of the investigated phthalocyanines were the ligands, and the torsions were assigned along the rotatable bonds. The binding constant K_B was calculated using the following equation:

$$K_B = e^{-\frac{\Delta G_B}{R \cdot T}},$$

where ΔG_B is the binding affinity (J·mol^{-1}), R is the gas constant (J·mol^{-1}·K^{-1}), and T is the temperature (298 K).

3. Results

3.1. Characterization of the Investigated Metal-Phthalocyanines

Energetic Parameters of the Metal-Phthalocyanines

According to data from the literature, a good sensitizer is characterized by a small HOMO–LUMO gap and lower energy of the HOMO frontier molecular orbital, both representing an advantage for electron transfer. Based on the results depicted in Tables 1–3, the compounds that fulfill both requirements are phthalocyanines substituted with amino groups (type I). The central metal has no influence on the values of the frontier molecular orbitals.

Table 1. HOMO orbital energies (a.u.) (HF/LanL2DZ level of theory).

Metal-Phthalocyanine	Type		
Metal	I (NH$_2$)	II (CH$_3$)	III (H)
Fe	−0.46178	−0.59676	−0.54731
Ni	−0.46883	−0.58613	−0.54393
Zn	−0.46707	−0.58437	−0.54284

Table 2. LUMO orbital energies (a.u.) (HF/LanL2DZ level of theory).

Metal-Phthalocyanine	Type		
Metal	I	II	III
Fe	−0.24888	−0.32408	−0.27515
Ni	−0.24706	−0.31478	−0.28272
Zn	−0.24645	−0.31631	−0.28205

Table 3. HOMO–LUMO gap (eV) (HF/LanL2DZ level of theory).

Metal-Phthalocyanine	Type		
Metal	I	II	III
Fe	5.79	7.42	7.40
Ni	6.03	7.38	7.10
Zn	6.00	7.29	7.09

The above results outline that the lowest-energy HOMO orbitals were obtained for type I metal-phthalocyanines (i.e., those substituted with amino groups), followed by type II (those substituted with methyl groups), while the smallest HOMO–LUMO differences are obtained for type I and III metal-phthalocyanines (those substituted with amino and unsubstituted, respectively). Regarding the influence of the metal, no common hierarchy can be established, as the values differ depending on the type of grafted substituents.

Graphical distribution of the HOMO orbitals was performed, with differences appearing among the investigated phthalocyanines. According to the results, the HOMO orbitals are localized as follows: for type I Zn and Ni phthalocyanines, they are localized at the phenyl rings and the corresponding amino group; for the Fe compound, they are asymmetrically localized at two of the four phenyl rings; concerning the type II phthalocyanines, the frontier molecular HOMO orbitals appear asymmetrically delocalized on the two or three phenyl rings; and for the type III phthalocyanines, they are symmetrical distributed on the four phenyl rings. It can be concluded that the presence of the substituents does not influence the energy of HOMO orbitals, which is in good agreement with the results presented in Table 1. The graphical distribution of the HOMO orbitals is presented in the Figure 3.
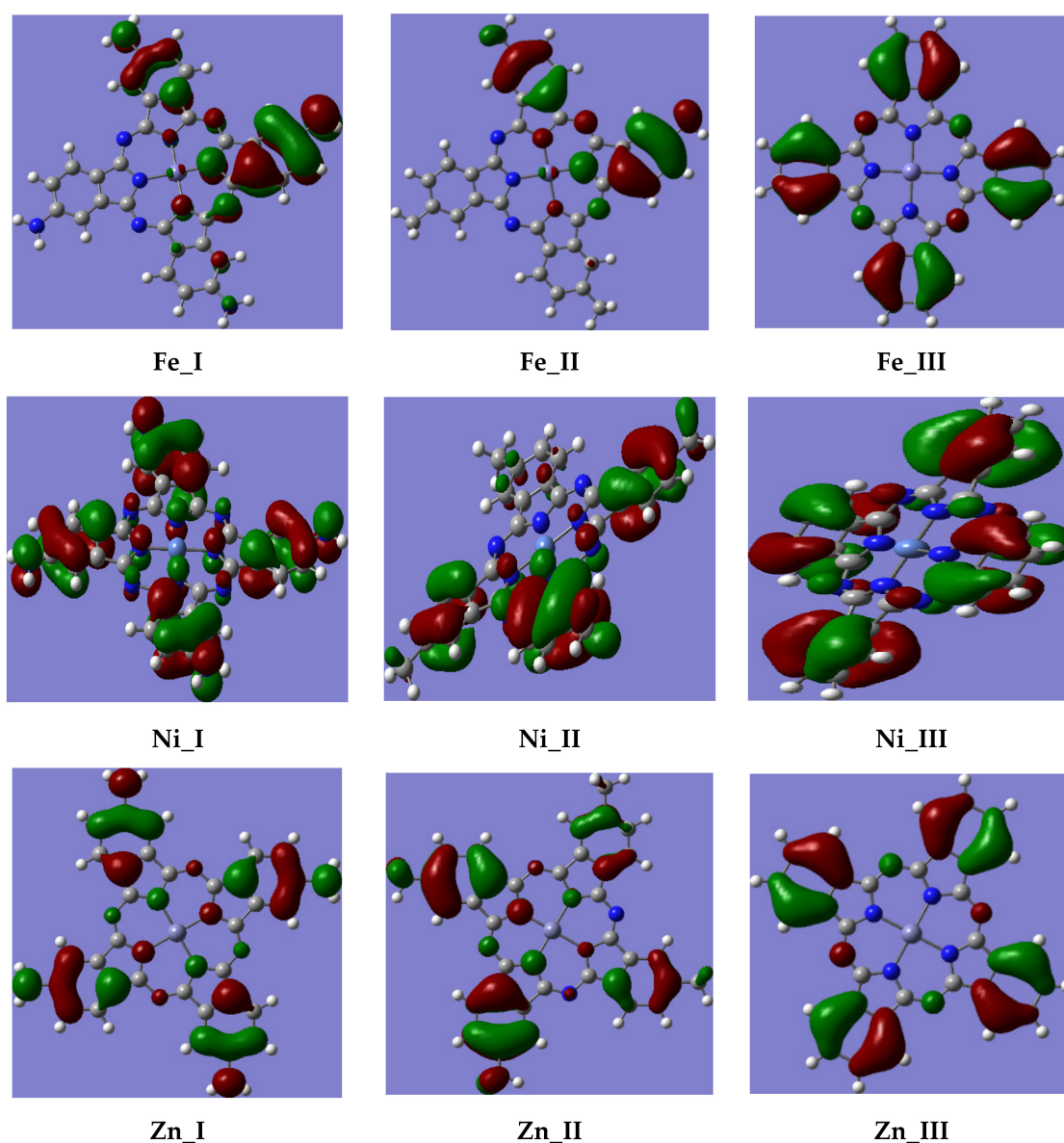

Figure 3. Graphical distribution of the HOMO orbitals of the metal-phthalocyanines.

The results depicted in Tables 1–3 suggest a similar behavior for nickel- and zinc-phthalocyanines. The geometry of the optimized structures shows that both structures have a bond length between nitrogen and metal of 1.88 Å, while a value of 1.97 Å is obtained for the Fe-phthalocyanines regardless the substitution type.

Using the frontier molecular energies, other global reactivity parameters were computed, with higher values of chemical potential, chemical hardness, and electrophilicity obtained for the metal-phthalocyanines substituted with methyl groups (type II). The results are depicted in Table 4. It can be observed that type II and III of the investigated compounds are characterized by similar values of chemical hardness.

Table 4. Chemical potential (μ), hardness (η), and electrophilicity (ω) (eV) (HF/LanL2DZ level of theory).

Metal-Phthalocyanine	Type								
Metal	I			II			III		
	μ	η	ω	μ	η	ω	μ	η	ω
Fe	−9.66	2.89	16.14	−12.52	3.71	21.12	−11.18	3.70	16.89
Ni	−9.74	3.02	15.71	−12.25	3.69	20.33	−11.24	3.55	17.79
Zn	−9.70	3.00	15.69	−12.25	3.65	20.56	−11.22	3.55	17.73

The graphical distribution of the HOMO orbitals is depicted in Figure 3.

3.2. Steric Parameters of the Metal-Phthalocyanines

Prior to the docking studies, a number of steric parameters, namely, the Connolly accessible area, Connolly solvent-excluded volume, and ovality, were computed. The results are presented in Tables 5–7. Molecular shape descriptors play an important role in elucidating the mechanisms of action in the field of drug design. The accessible surface is often used to calculate the free transfer energy required to transfer a molecule from an aqueous solvent to a non-polar solvent such as a lipid environment. Connolly Accessible Area (CAA) is defined as the locus of the center of the solvent as it is rolled over the molecular model [24]. The Connolly Solvent-Excluded Volume (CSEV) represents the volume contained within the contact molecular surface [24]. The ovality estimates the degree of deviation from the spheric shape.

Table 5. Connolly accessible area values (Å^2).

Metal-Phthalocyanine	Type		
Metal	I	II	III
Fe	828.137	857.177	746.368
Ni	807.502	831.380	734.398
Zn	807.228	831.103	734.125

Table 6. Connolly solvent-excluded volume (Å^3).

Metal-Phthalocyanine	Type		
Metal	I	II	III
Fe	446.658	463.648	401.310
Ni	452.146	466.770	407.765
Zn	450.573	465.204	406.192

Table 7. Ovality.

Metal-Phthalocyanine	Type		
Metal	I	II	III
Fe	1.65	1.73	1.60
Ni	1.65	1.67	1.60
Zn	1.65	1.67	1.60

These results outline the geometric similarities between the nickel and zinc phthalo-cyanins as predicted by the same nitrogen-metal bond length. Regarding the influence of the substituents, the presence of the methyl groups leads to larger values for the solvent accessible area and ovality.

The lowest values of the ovality, which is defined as the deviation from the spherical shape, were obtained for the unsubstituted metal-phthalocyanins.

3.3. Other Properties of the Metal-Phthalocyanins: logP, Dipole Moment, Wavelength of Maximum Absorbance

The results of our computational calculations show that a higher hydrophobic charac-ter was obtained for the iron phthalocyanines (see Table 8). Regarding the influence of the substituents, as expected, the methyl derivatives are characterized by the highest values of the partition coefficient.

Table 8. Computed partition coefficient (logP).

Metal-Phthalocyanine	Type		
Metal	I	II	III
Fe	2.87	12.90	10.83
Ni	0.94	10.96	8.89
Zn	0.82	10.84	8.77

Other important parameters that characterize the photosensitizers are the dipole mo-ment and the UV–Vis absorption within the 400–650 nm range. According to the calculated UV spectra for the investigated metal-phthalocyanines, the wavelength of maximum ab-sorbance lies within the 522–599 nm. The condition of a low dipole moment is fulfilled as well, with the majority of the metal-phthalocyanins being characterized by a zero-dipole moment. The results are included in Tables 9 and 10.

Table 9. Computed wavelengths Λ_{max} (nm).

Metal-Phthalocyanine	Type		
Metal	I	II	III
Fe	529	541	559
Ni	538	522	553
Zn	576	599	555

Table 10. Computed dipole moment (D).

Metal-Phthalocyanine	Type		
Metal	I	II	III
Fe	2.68	2.79	0
Ni	0	0	0
Zn	0	0.82	0

3.4. Molecular Docking Studies

Various carbon-based nanomaterials have been successfully used as delivery systems for both hydrophobic and hydrophilic compounds. In the present study, four fullerenes consisting of 52 atoms were chosen (all-carbon C_{52} and Three aza-phospha-fullerenes" instead of "fullerenes doped with nitrogen and phosphorus atoms, $C_{46}N_3P_3$).

Prior to the docking studies, a short characterization of the fullerenes was performed using the same level of theory as for the metal-phthalocyanines (HF/LanL2DZ).

The results depicted in Tables 11 and 12 outline only small differences regarding the stability of the fullerenes, the most stable (as indicated by the HL gap) being C_{52}. The presence of the six heteroatoms leads to an increase polarity of the surface for the $C_{46}N_3P_3$ fullerenes.

Table 11. Frontier molecular orbital energies and computed HOMO-LUMO gap (HF/LanL2DZ).

Compounds	E $_{HOMO}$ (H)	E $_{LUMO}$ (H)	HOMO-LUMO gap (eV)
C_{52}	−0.2572	−0.0841	4.708
$C_{46}N_3P_3$(A)	−0.2107	−0.0772	3.631
$C_{46}N_3P_3$(B)	−0.1770	−0.0441	3.615
$C_{46}N_3P_3$(C)	−0.1859	−0.0551	3.558

Table 12. Topological characterization of the fullerenes.

Compounds	Polar Surface Area	Shape Attribute	Topological Diameter
C_{52}	0	50.02	8 bonds
$C_{46}N_3P_3$(A)	9.72	50.02	8 bonds
$C_{46}N_3P_3$(B)	9.72	50.02	8 bonds
$C_{46}N_3P_3$(C)	9.72	50.02	8 bonds

The molecular docking studies with the metal-phthalocyanins considered as ligands and the fullerenes as receptors led to the results presented below. The intermediate binding affinities are depicted in Tables 13–16, while the best binding affinities of ligands with the nanostructures are presented in Tables 17 and 18.

Table 13. Binding affinity for metal-phthalocyanines with $C_{46}N_3P_3$ (A) for nine conformations (kcal/mol).

	E1	E2	E3	E4	E5	E6	E7	E8	E9
Fe_I	−6.2	−6.2	−6.2	−6.2	−6.2	−6.2	−6.2	−−6.2	−6.1
Fe_II	−6.8	−6.8	−6.7	−6.7	−6.7	−6.7	−6.7	−6.7	−6.7
Fe_III	−6.5	−6.5	−6.5	−6.4	−6.4	−6.4	−6.4	−6.4	−6.4
Ni_I	−6.4	−6.4	−6.4	−6.4	−6.3	−6.3	−6.3	−6.3	−6.3
Ni_II	−7.1	−7.1	−7.1	−7.1	−7.1	−7.1	−7.1	−7.1	−7.1
Ni_III	−6.9	−6.9	−6.9	−6.9	−6.9	−6.9	−6.9	−6.9	−6.9
Zn_I	−6.4	−6.4	−6.4	−6.4	−6.4	−6.3	−6.3	−6.3	−6.3
Zn_II	−7.1	−7.1	−7.1	−7.1	−7.1	−7.1	−7.1	−7.0	−7.0
Zn_III	−7.0	−6.9	−6.9	−6.9	−6.9	−6.9	−6.9	−6.9	−6.9

Table 14. Binding affinity for metal-phthalocyanines with $C_{46}N_3P_3$ (B) for nine conformations (kcal/mol).

	E1	E2	E3	E4	E5	E6	E7	E8	E9
Fe_I	−6.2	−6.2	−6.2	−6.2	−6.2	−6.2	−6.2	−6.2	−6.1
Fe_II	−6.7	−6.7	−6.7	−6.7	−6.7	−6.7	−6.7	−6.7	−6.7
Fe_III	−6.5	−6.5	−6.5	−6.5	−6.5	−6.5	−6.5	−6.5	−6.5
Ni_I	−6.4	−6.4	−6.4	−6.4	−6.4	−6.4	−6.3	−6.3	−6.3
Ni_II	−7.1	−7.1	−7.1	−7.1	−7.1	−7.1	−7.1	−7.1	−7.1
Ni_III	−7.0	−6.9	−6.9	−6.9	−6.9	−6.9	−6.9	−6.9	−6.9
Zn_I	−6.4	−6.4	−6.4	−6.4	−6.4	−6.4	−6.3	−6.3	−6.3
Zn_II	−7.1	−7.1	−7.1	−7.1	−7.1	−7.1	−7.1	−7.1	−7.1
Zn_III	−7.0	−6.9	−6.9	−6.9	−6.9	−6.9	−6.9	−6.9	−6.9

Table 15. Binding affinity for metal-phthalocyanines with $C_{46}N_3P_3$ (C) for nine conformations (kcal/mol).

	E1	E2	E3	E4	E5	E6	E7	E8	E9
Fe_I	−6.2	−6.2	−6.2	−6.2	−6.2	−6.2	−6.2	−6.1	−6.1
Fe_II	−6.8	−6.8	−6.7	−6.7	−6.7	−6.7	−6.7	−6.7	−6.7
Fe_III	−6.5	−6.5	−6.5	−6.5	−6.5	−6.5	−6.5	−6.5	−6.5
Ni_I	−6.4	−6.4	−6.4	−6.4	−6.3	−6.3	−6.3	−6.3	−6.3
Ni_II	−7.1	−7.1	−7.1	−7.1	−7.1	−7.1	−7.1	−7.1	−7.1
Ni_III	−7.0	−6.9	−6.9	−6.9	−6.9	−6.9	−6.9	−6.9	−6.9
Zn_I	−6.4	−6.4	−6.4	−6.4	−6.4	−6.4	−6.4	−6.3	−6.3
Zn_II	−7.1	−7.1	−7.1	−7.1	−7.1	−7.1	−7.1	−7.1	−7.1
Zn_III	−7.0	−7.0	−7.0	−6.9	−6.9	−6.9	−6.9	−6.9	−6.9

Table 16. Binding affinity for metal-phthalocyanines with C_{52} for nine conformations (kcal/mol).

	E1	E2	E3	E4	E5	E6	E7	E8	E9
Fe_I	−6.2	−6.2	−6.2	−6.2	−6.2	−6.2	−6.2	−6.2	−6.2
Fe_II	−6.8	−6.8	−6.7	−6.7	−6.7	−6.7	−6.7	−6.7	−6.7
Fe_III	−6.5	−6.5	−6.5	−6.5	−6.5	−6.5	−6.5	−6.5	−6.5
Ni_I	−6.4	−6.4	−6.4	−6.4	−6.4	−6.3	−6.3	−6.3	−6.3
Ni_II	−7.2	−7.1	−7.1	−7.1	−7.1	−7.1	−7.1	−7.1	−7.1
Ni_III	−7.0	−7.0	−7.0	−7.0	−6.9	−6.9	−6.9	−6.9	−6.9
Zn_I	−6.4	−6.4	−6.4	−6.4	−6.4	−6.4	−6.4	−6.3	−6.3
Zn_II	−7.2	−7.1	−7.1	−7.1	−7.1	−7.1	−7.1	−7.1	−7.1
Zn_III	−7.0	−7.0	−6.9	−6.9	−6.9	−6.9	−6.9	−6.9	−6.9

Table 17. The final Lamarckian genetic algorithm docked state: best binding affinities of ligands with the nanostructures (kcal mol^{-1}).

Compound	Fe-PTC			Ni-PTC			Zn-PTC		
	I	II	III	I	II	III	I	II	III
C_{52}	−6.20	−6.72	−6.50	−6.34	−7.11	−6.94	−6.37	−7.11	−6.92
$C_{46}N_3P_3$ (A)	−6.18	−6.72	−6.43	−6.34	−7.10	−6.90	−6.35	−7.08	−6.91
$C_{46}N_3P_3$ (B)	−6.19	−6.70	−6.50	−6.37	−7.10	−6.91	−6.36	−7.10	−6.91
$C_{46}N_3P_3$ (C)	−6.17	−6.72	−6.50	−6.34	−7.10	−6.91	−6.38	−7.10	−6.93

Table 18. Calculated constant binding K_B ($\cdot 10^4$).

Compound	Fe-PTC			Ni-PTC			Zn-PTC		
	I	II	III	I	II	III	I	II	III
C_{52}	3.53	8.49	5.85	4.55	16.40	12.31	4.70	16.40	11.89
$C_{46}N_3P_3$ (A)	3.53	8.49	5.20	4.47	16.12	11.50	4.54	15.33	11.50
$C_{46}N_3P_3$ (B)	3.53	8.21	5.85	4.62	16.12	11.50	4.62	16.12	11.50
$C_{46}N_3P_3$ (C)	3.35	8.49	5.85	4.47	16.12	11.50	4.70	16.12	12.10

The main conclusions regarding the interactions between each metal-phthalocyanine and the corresponding fullerene structure are the following:

(i). Regardless of the type of fullerene, the best binding affinities were obtained for the metal-phthalocyanines substituted with methyl groups, followed by the unsubstituted structures. The only type of interaction that of atoms in close-contact, with no hydrogen bonds being established;

(ii). Concerning the influence of the central metal, among the investigated phthalocyanines the lowest binding constants were obtained for Fe-PTC. No significant difference between Ni-PTC and Zn-PTC could be determined;

(iii). Considering that the best results were obtained for the type II and III phthalocyanines, which are those characterized by higher values of the partition coefficient, it can be said that the hydrophobicity of the compounds is the most important parameter in obtaining higher binding affinities and binding constants.

4. Discussion

The present paper has dealt with the investigation of the properties of iron-, nickel- and zinc-phthalocyanines as possible photosensitizers. In this regard, we computed several properties, including the HOMO–LUMO gap value, dipole moment, and wavelength of maximum absorbance, with the results suggesting that all of the investigated compounds possess the requirements of good photosensitizers.

Concerning the influence of the central metal on the properties of the studied compounds, the following conclusions can be stated:

(i). The energies of the frontier molecular orbitals HOMO and LUMO are very slightly influenced by the type of the metal; as a result, the calculated global reactivity parameters presented in Tables 1–4 have similar values among the same substitution type, regardless of whether the metal is iron, nickel, or zinc;

(ii). The central metal influences the steric parameters of the phthalocyanines, with a larger nitrogen-iron bond (1.97 Å, compared to 1.88 Å for nickel- and zinc-nitrogen) leading to different values of the Connolly Accessible Area and Connolly Solvent-Excluded Volume for iron-phthalocyanines on the one hand and nickel- and zinc-phthalocyanines on the other.

The main influence on the properties of the metal-phthalocyanines arises from the presence of the substituents. The differences are outlined in the calculated reactivity descriptors depicted in Tables 1–4. It can be observed that the presence of the methyl groups leads to higher energies for the HOMO and LUMO orbitals, while the amino-substituted compounds are characterized by lower energies as compared to unsubstituted metal-phthalocyanines.

Another part of the present study dealt with the interactions between each metal-phthalocyanine and four fullerenes consisting of 52 atoms (one all-carbon and three fullerenes doped with isovalent nitrogen and phosphorus atoms) as possible delivery systems. The best affinities were obtained for the phthalocyanines substituted with methyl groups and where the central metal was Ni and Zn.

Based on the calculated properties, the characteristics of the ideal metal-phthalocyanines within the investigated series are those shown in Table 19.

Table 19. Characteristics of the metal-phthalocyanins with highest affinity for fullerenes.

logP	ΔHL	Dipole Moment	Ovality	CAA	CSEV
~10–11	~7.30–7.40 eV	~0	1.67	830–832 $Å^2$	465–467 $Å^3$

References

1. Triesscheijn, M.; Baas, P.; Schellens, J.; Stewart, F. Photodynamic therapy in oncology. *Oncologist* **2006**, *11*, 1034–1044. [CrossRef] [PubMed]
2. Gunaydin, G.; Gedik, E.; Ayan, S. Photodynamic therapy for the treatment and diagnosis of cancer—A review of the current clinical status. *Front. Chem.* **2021**, *9*, 686303. [CrossRef] [PubMed]
3. Lo, P.-C.; Rodriguez-Morgade, S.; Pandey, R.; Ng, D.; Torres, T.; Dumoulin, F. The unique features and promises of phthalocyanines as advanced photosensitisers for photodynamic therapy of cancer. *Chem. Soc. Rev.* **2020**, *49*, 1041–1056. [CrossRef] [PubMed]
4. Baron, E.; Malbasa, C.; Santo-Domingo, D.; Fu, P.; Miller, J.D.; Hanneman, K.K.; Hsia, A.H.; Oleinick, N.L.; Collusi, V.C.; Cooper, K.D. Silicon phthalocyanine (Pc 4) photodynamic therapy is a safe modality for cutaneous neoplasms: Results of phase 1 clinical trial. *Lasers Surg. Med.* **2010**, *42*, 728–735. [CrossRef] [PubMed]
5. Zheng, B.-Y.; Wang, L.; Hu, Q.-Y.; Shi, J.; Ke, M.R.; Huang, J.D. Novel unsymmetrical silicon(IV) phthalocyanines as highly potent anticancer photosensitizers. Synthesis, characterization, and in vitro photodynamic activities. *Dye. Pigment.* **2020**, *177*, 108286. [CrossRef]
6. Roguin, L.; Chiarante, N.; Vior, M.; Marino, J. Zinc(II) phthalocyanines as photosensitizers for antitumor photodynamic therapy. *Int. J. Biochem. Cell Biol.* **2019**, *114*, 105575. [CrossRef]
7. Crous, A.; Abrahamse, H. Aluminium(III) phthalocyanine chloride tetrasulphonate is an effective photosensitizer for the eradication of lung cancer stem cells. *R. Soc. Open Sci.* **2021**, *8*, 210148. [CrossRef]
8. Jia, X.; Jia, L. Nanoparticles improve biological functions of phthalocyanine photosensitizers used for photodynamic therapy. *Curr. Drug Metab.* **2012**, *13*, 1119–1122. [CrossRef]
9. Zhong, A.; Zhang, Y.; Bian, Y. Structures and spectroscopic properties of nonperipherally and peripherally substituted metal-free phthalocyanines: A substitution effect study based on density functional theory calculations. *J. Mol. Graph. Model.* **2010**, *29*, 470–480. [CrossRef]
10. Ozcesmeci, I.; Tekin, A.; Gul, A. Synthesis and aggregation behavior of zinc phthalocyanines substituted with bulky naphthoxy and phenylazonaphthoxy groups: An experimental and theoretical study. *Synth. Met.* **2014**, *189*, 100–110. [CrossRef]
11. Akcay, T.H.; Bayrak, R.; Karslioglu, S.; Sahin, E. Synthesis, characterization and spectroscopic studies of novel peripherally tetra-imidazole substituted phthalocyanine and its metal complexes, the computational and experimental studies of the novel phthalonitrile derivative. *J. Organomet. Chem.* **2012**, *713*, 1–10. [CrossRef]
12. Ocakoglu, K.; Er, O.; Ersoz, O.A.; Lambrecht, F.Y.; Ince, M.; Kayabasi, C.; Gunduz, C. Evaluation of nuclear imaging potential and photodynamic therapy efficacy of symmetrical and asymmetrical zinc phthalocyanines. *J. Drug Deliv. Sci. Technol.* **2016**, *33*, 164–169. [CrossRef]
13. Pucelik, B.; Gurol, I.; Ahsen, V.; Dumoulin, F.; Dabrowski, J.M. Fluorination of phthalocyanine substituents: Improved photoproperties and enhanced photodynamic efficacy after optimal micellar formulations. *Eur. J. Med. Chem.* **2016**, *124*, 284–298. [CrossRef] [PubMed]
14. Milcovich, G.; Antunes, F.; Golob, S.; Farra, R.; Grassi, M.; Voinovich, D.; Grassi, G.; Asaro, F. Thermo-responsive hydrogels from cellulose-based polyelectrolytes and catanionic vesicles for biomedical application. *J. Biomed. Mater. Res. Part A* **2016**, *104*, 1668–1679. [CrossRef] [PubMed]

15. Py-Daniel, K.R.; Namban, J.S.; de Andrade, L.R.; de Souza, P.E.N.; Paterno, L.G.; Azevedo, R.B.; Soler, M.A.G. Highly efficient photodynamic therapy colloidal system based on chloroaluminum phthalocyanine/pluronic micelles. *Eur. J. Pharm. Biopharm.* **2016**, *103*, 23–31. [CrossRef]
16. Liu, J.Y.; Li, J.; Yuan, X.; Wang, W.M.; Xue, J.P. In vitro photodynamic activities of zinc(II) phthalocyanines substituted with pyridine moieties. *Photodiagnosis Photodyn. Ther.* **2016**, *13*, 341–343. [CrossRef]
17. Cakir, D.; Cakir, V.; Biyiklioglu, Z.; Durmus, M.; Kantekin, H. New water soluble cationic zinc phthalocyanines as potential for photodynamic therapy of cancer. *J. Organomet. Chem.* **2013**, *745*, 423–431. [CrossRef]
18. Abrahamse, H.; Hamblin, M.R. New photosensitizers for photodynamic therapy. *Biochem. J.* **2016**, *473*, 347–364.
19. Pop, R.; Andoni, M.; van Staden, J.; Medeleanu, M.; Pausescu, I. Theoretical considerations regarding the aromaticity of ∧3-heterobenzenes containing 15-group elements. *Dig. J. Nanomater. Biostruct.* **2013**, *8*, 1739–1750.
20. Pop, R.; van Staden, J.; Diudea, M. Nitrogen-Containing Coronenes: Theoretical Evaluation of the Influence of Aza-substitution on their Aromaticity. *Z. Für Nat. A* **2015**, *70*, 171–175. [CrossRef]
21. Frisch, M.J.; Trucks, G.W.; Schlegel, H.B.; Scuseria, G.E.; Robb, M.A.; Cheeseman, J.R.; Scalmani, G.; Barone, V. *Gaussian 09*, Revision B.01; Gaussian, Inc.: Wallingford, CT, USA, 2010.
22. Zyrianov, Y. Distribution-based descriptors of the molecular shape. *J. Chem. Inf. Model.* **2005**, *45*, 657–672. [CrossRef] [PubMed]
23. Trott, O.; Olson, A.J. AutoDock Vina: Improving the speed and accuracy of docking with a new scoring function, efficient optimization, and multithreading. *J. Comput. Chem.* **2010**, *31*, 455–461. [CrossRef] [PubMed]
24. Connolly, M.L. The Molecular Surface Package. *J. Mol. Graph.* **1993**, *11*, 139–141. [CrossRef]